SELF-PIXELATION THROUGH FRACTURE IN VO_2 THIN FILMS

Laura Rodríguez,[*,§,‡] *Elena del Corro,*[§] *Michele Conroy,*[†] *Kalani Moore,*[†] *Felip Sandiumenge,*[⊥] *Neus Domingo,*[§] *José Santiso,*[§] *and Gustau Catalan*[§,¥]

§ Institut Català de Nanociència i Nanotecnologia (ICN2), CSIC and The Barcelona Institute of Nanoscience and Technology (BIST), Campus UAB, 08193 Barcelona, Catalonia, Spain.

‡ Departament de Física Aplicada, Facultat de Física, Universitat de Barcelona (UB), 08028 Barcelona, Catalonia, Spain.

† TEMUL, Department of Physics, School of Natural Sciences & Bernal Institute, University of Limerick, AD3-009 Limerick, Ireland.

⊥ Institut de Ciència de Materials de Barcelona, ICMAB-CSIC, Campus de la UAB, 08193 Barcelona, Catalonia, Spain.

¥ ICREA-Institució Catalana de Recerca i Estudis Avançats, 08010 Barcelona, Catalonia.

I. ABSTRACT

Vanadium dioxide (VO_2) is an archetypal Mott material with a metal-insulator transition (MIT) near room temperature. In thin films, this transition is affected by substrate-induced strain but, as film thickness increases, the strain is gradually relaxed and the bulk properties are recovered. Epitaxial films of VO_2 on (001)-oriented rutile titanium dioxide (TiO_2) relax substrate strain by forming a network of fracture lines that crisscross the film along well-defined crystallographic directions. This work shows that the electronic properties associated with these lines result in a pattern that resembles a "street map" of fully strained metallic VO_2 blocks separated by insulating VO_2 stripes. Each block of VO_2 is thus electronically self-insulated from its neighbors and its MIT can be locally induced optically with a laser, or electronically via the tip of a scanning probe microscope, so that the films behave functionally as self-patterned pixel arrays.

KEYWORDS: Metal-insulator transition, thin-films, vanadium dioxide, cracks, pixelation, scanning Kelvin probe microscopy.

II. INTRODUCCTION

Vanadium dioxide (VO_2) is a reference material for the study of metal-insulator transitions (MIT).[1-6] Its MIT is sharp, with a resistance change of several orders of magnitude accompanied by a visible change of optical properties, and it happens close to room temperature (RT), making it attractive for device applications.[3,6-11] The RT ground state of VO_2 is monoclinic, the so-called M1 polymorph, and electrically insulating (more accurately, semiconducting) with a bandgap around 0.6-0.8 eV.[1,10,12-15] Above the critical temperature of ~68 °C, VO_2 changes to a higher

symmetry rutile (R) form, which is tetragonal and metallic. Because the structural phase transition is coupled to the electronic transition,[13] it is possible to use epitaxial strain to modify the electronic properties and MIT of VO_2 thin films.[16-20]

Rutile titanium dioxide (R-TiO_2) is isostructural with the high-temperature metallic phase of VO_2 and has a sufficiently small lattice mismatch (see **Table 1**) to allow coherent growth of fully strained films. The substrate-induced strain favors the rutile structure of VO_2 (R-VO_2) which is metallic, thus lowering the critical temperature of the metal-insulator transition (T_{MI}). For films thicker than ~15 nm, however, the strain starts to be relaxed.[21] What is unusual in VO_2 is the manner in which this strain relaxation proceeds: instead of generating dislocations, the biaxial stress is relaxed by fracturing.[21,22]

The sudden volume contraction and change of symmetry experienced by VO_2 across its first-order MIT is directly related to its structural response to stress, and cracking and/or heavy twinning have been observed in samples of any morphology, ranging from epitaxial thin films,[21,22] polycrystalline thin films,[23] polycrystalline membranes –which tend to crack along grain boundaries[24] and even free-standing single crystals, which fracture after several heating-cooling cycles.[25] Since the strain state around cracks is inhomogeneous,[26,27] the local phase stability and electronic properties may be very different near the cracks than away from them. That expected difference is the starting premise for the present investigation.

In this work, we have studied the structural and electronic properties of VO_2 thin films at the nanoscale, focusing on the interplay between the phase transition and the strain relaxation pattern. Epitaxial single-crystalline films of VO_2 are atomically flat and have no grain boundaries, providing a very clean system both for the propagation of cracks and for their

ulterior characterization by scanning probe microscopy techniques –which allow studying their functional as well as structural properties. We find that strain relaxation proceeds through the appearance of a lattice of straight cracks along the $<110>_R$ crystallographic directions, decorated by insulating VO_2 strips and bounding square tiles of fully strained VO_2. The result resembles an irregular tiling or an array of streets and blocks reduced to the nanoscale, with distinct electronic properties associated with each feature.

As we show, the MIT can be induced in these islands by illuminating or injecting charge in them with the tip of an atomic force microscope. This structure behaves de facto as a pixel array, making it possible to individually write and read each VO_2 "bit" (strained island) without affecting its neighbors in ultrafast switching times (from hundreds of picoseconds in the case of photoinduced MIT[28] to nanoseconds in devices based on voltage-induced MIT[29]).

III. EXPERIMENTAL

VO_2 films were grown by Pulsed Laser Deposition (PLD) with thicknesses between 5 and 120 nm. X-ray Diffraction (XRD) and Reciprocal Space Maps (RSMs) were used to characterize the structural features of the samples. Macroscopic electrical transport measurements as a function of temperature were done in a cryostat in 4-probe Van-der-Pauw configuration. Surface topography and microstructure were characterized by Atomic Force Microscopy (AFM) and Scanning Electron Microscopy (SEM), while the cross-sectional aspect of the strain relaxation was characterized by High Resolution Transmission Electron Microscopy (HRTEM). Optical microscopy and micro-Raman spectroscopy were used to visualize the optical and structural

evolution across the metal-insulator transition. The nanoscale dependence of local electronic properties on temperature and voltage was studied by means of Scanning Kelvin Probe Microscopy (SKPM) using a Pt/Ir conductive-tip atomic force microscope. A detailed description of the experimental methods is given in the Supplementary Information (see supplementary experimental details).

IV. RESULTS AND DISCUSSION

X-ray diffraction (XRD) confirms the phase purity and epitaxy of the films (see Supporting Information **Figure S1**). The temperature evolution of the 002_R diffraction peak (**Figure 1** and **Figure S2**) shows a switch from the monoclinic phase (longer out-of-plane lattice parameter) to the rutile phase (shorter out-of-plane lattice parameter) as temperature increases; the crystallographic information about the parent bulk phases is summarized in **Table 1**. The process is reversible upon cooling, and the critical temperature depends on thickness. At RT, films thinner than ~ 35 nm are rutile while those above ~ 85 nm are mostly relaxed into the monoclinic phase (**Figure S2**). In the intermediate range, rutile and monoclinic peaks are simultaneously present at RT, indicating phase coexistence.

In **Figure 1** we compare the relative volume fraction of rutile (metallic) phase with the resistance as a function of temperature measured simultaneously for the same film. This comparison yields the first indication that the macroscopic properties cannot be explained without access to the local microscopic behavior. Specifically, the result shows that more than 95% of the film needs to be in the rutile (metallic) phase before undergoing the electronic transition to macroscopically metallic transport. Such a high percolation threshold is not

consistent with mean-field behavior, as random-bond models have much lower critical percolation thresholds of 1/3 (in 3D) or 1/2 (in 2D).[30]

Table 1. Comparison of R-TiO_2, R-VO_2 and M1-VO_2 structural parameters.

		LATTICE PARAMETERS (Å)			ANGLES (º)			MISMATCH (%)	REFERENCE
	Space Group	a	b	c	α	β	γ	In-plane	ICSD Code
R-TiO_2	*P4$_2$/mnm* (136)	4.594	4.594	2.959	90	90	90	-	23697
R-VO_2	*P4$_2$/mnm* (136)	4.555	4.555	2.851	90	90	90	+0.9	4110
M1-VO_2	*P12$_1$/c1* (14)	5.743	4.517	5.375	90	122.61	90	+1.7(b_{M1}); +1.4(c_{M1})	15889
(in pseudo-R cell)		(4.517)	(4.528)	(2.872)					

The substrate, R-TiO_2, induces in-plane tensile strain in both R-VO_2 and M1-VO_2, but the lattice mismatch is smaller with respect to R-VO_2 and hence the metallic phase is favored, so T_{MI} is lower for fully strained films than for bulk. The M1-VO_2 structure is also expressed in the rutile reference frame to facilitate comparison with the substrate lattice parameters.

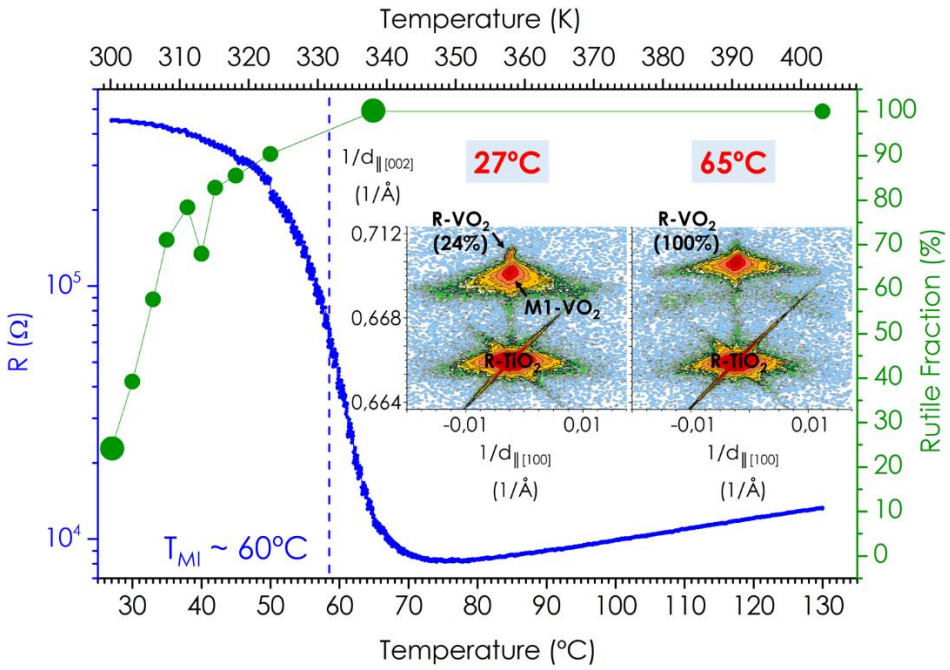

Figure 1. Macroscopic electrical transport and the structural phase transition as a function of temperature for a VO_2 film of 85 nm. Resistance (blue line) was measured simultaneously with the collection of x-ray reciprocal space maps (RSM) around the 002_R reflexion, two examples of which are shown in the inset. The discontinuous vertical line marks the temperature at which d(logR)/dT is maximum, corresponding to the percolative T_{MI} in the electronic transport.[30] The relative volumes of monoclinic and rutile phase (green) were extracted from the integrated intensities of the X-ray peaks. Bigger symbols are used to mark the data corresponding to the two representative maps (insets); a supplementary video runs through the complete set of resistivity and diffraction measurements as a function of temperature for both heating and cooling (see SV.1).

AFM shows that, while films thinner than ~15 nm are continuous (**Figure 2**a), thicker films display a rectangular pattern of ridges parallel to the $<110>_R$ crystallographic directions (**Figure**

2b). SEM (**Figure S3**) reveals that these ridges correspond to the edges of cracks that are <10 nm in width. The images also show that the number of cracks increases with thickness (**Figure S3**), consistent with cracking being the main stress-relieving mechanism of the films.[21]

Cross-sectional TEM adds additional information. **Figure 2**c shows a HRTEM image of a crack seen edge-on (i.e. along the $[110]_R$ direction). Structural contrast can be observed within ~5 nm at each side of the crack, extending through the whole thickness of the film. A high-resolution close-up (**Figure S4**) reveals the structure adjacent to the crack to be consistent with insulating M1-VO_2,[5,31-33] with the matrix being rutile. The fact that the films are still macroscopically conducting despite the presence of cracks that are deep enough to reach the substrate suggests that either some of the cracks do not quite reach the bottom interface, or else they are so narrow near the base to allow for tunneling, thus acting as resistors in series with the bulk of the film.

Electron Energy Loss Spectroscopy (EELS) was also used to gain information on O and V states through the O-K (1s → 2p) and V-L (2p → 3d) core edges. In particular, the O-K edge probing the unoccupied O p density of states (shown in **Figure 2**d), is sensitive to the dimerization of V ions through the strong p-d hybridization.[31-33] Comparison between the two spectra shows that the transition across the interface towards the crack is accompanied by a drop in the intensity of the π^* band and a shift of ~ 0.2 eV towards higher energy particularly visible in the σ^* band (see also **Figure S5**). Both features are characteristic of the MIT.[31] The microscopic analysis therefore suggests that (i) epitaxial strain is relieved through a self-

patterned network of clean fissures along the <110>$_R$ directions and (ii) the cracks are decorated by a phase that is structurally and electronically distinct from the rest of the film.

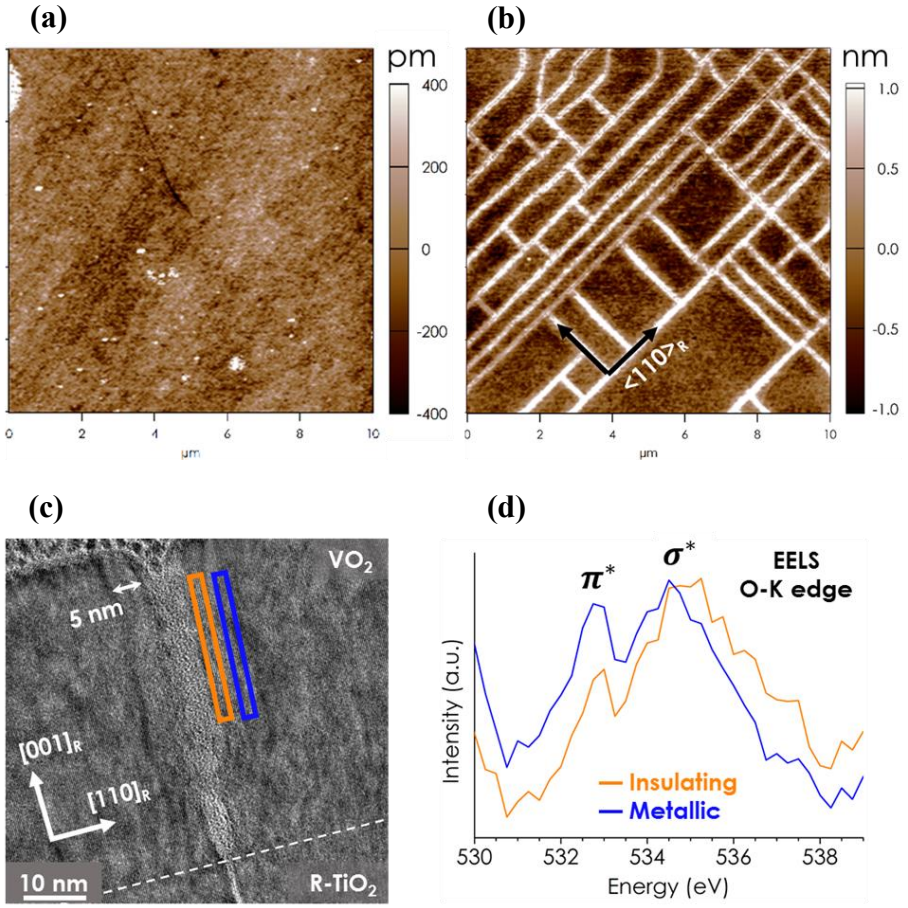

Figure 2. Crack patterning and crack-induced MIT. 10x10 μm AFM topography images of a (a) 10 nm film showing a continuous surface, and (b) a thicker film (60 nm) revealing a rectangular fracture pattern. (c) HRTEM cross-section viewed along the $[110]_R$ zone axis showing structural contrast near the crack-edges through the whole film thickness. (d) O-K EEL spectra obtained from the windows placed near the crack-edge (orange) and farther into the rutile phase (blue), as indicated in (c). These EELS spectra are consistent with the insulating and metallic phases of VO_2.

Given the correlation between structural, electronic and optical properties in VO_2, the local strain relaxation around the cracks may lead to optically visible contrasts. Optical microscopy and micro-Raman spectroscopy (**Figure 3**) bears this, and shows R-metallic rectangles (dark) framed by M1-insulating edges (pale) following the cracks. The unusually high percolation threshold in **Figure 1** is thus explained; since the cracks percolate across the entire surface of the film, if the cracks are decorated by insulating VO_2, the films will still behave macroscopically as insulators even if most of the volume (comprised by the islands) is metallic. Only when the strain-relaxed near-crack regions have also transitioned into the metallic state (at a higher temperature than the fully strained rutile islands) will there be metallic percolation.

The local transition temperature within each VO_2 "tile" depends on its local strain state, which in turn depends on it size and shape. Since the main strain-relaxation mechanism is cracking, smaller tiles where the cracks are closer together are more relaxed and thus tend to have a higher local T_{MI} (i.e., closer to the bulk transition temperature) while larger tiles tend to be more fully strained and have a lower T_{MI} (i.e. they remain metallic down to lower temperatures).

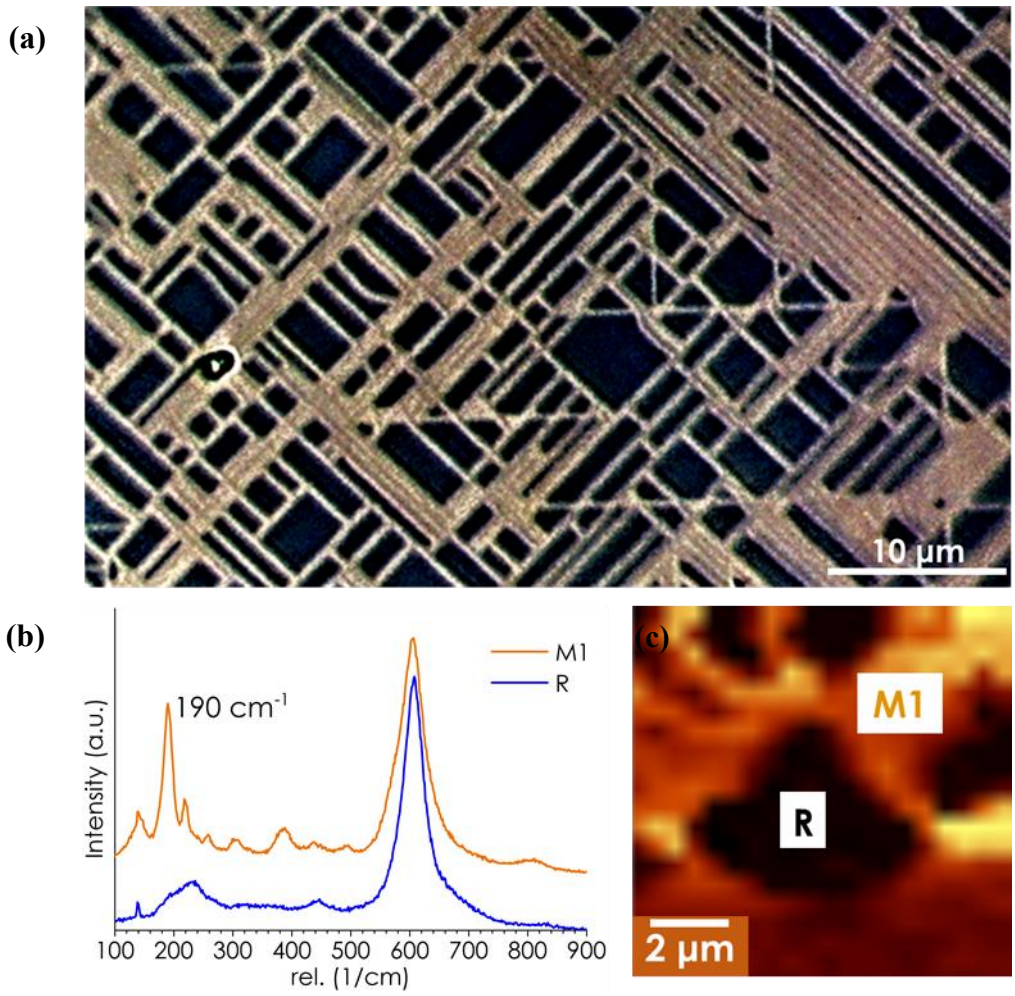

Figure 3. Insulating-M1 phase surrounding the cracks. (a) Optical image using natural light showing the difference in contrast of metallic-R domains (darker domains) and the insulating near-crack regions (brighter areas). (b) Micro-Raman spectroscopy correlating the R and M1 structures with the inner region of a domain and the near-crack region framing the domain, respectively. The M1-VO_2 peak around 190 cm^{-1} (b) was used to map (c) the M1 presence (yellowish color) or its absence (black).

The local electronic properties were also examined by means of temperature-dependent SKPM, which measures differences in work-function between the surface of the film and the

metallic tip. The absolute value of the surface potential is a delicate magnitude that depends on surface chemistry, which is sensitive to defects and adsorbates. Its relative changes, however, are a good proxy for the metal-insulator transition.[34-37] **Figure 4**a shows the SKPM maps of a film of 20 nm grown on a conductive substrate of Nb-doped TiO_2(001) connected to bias in this case, with scans at three representative temperatures of the experiment. The height scale is common for the 3 images showing no topography changes across the MIT. The false color scale is chosen so that blue represents a lower absolute value of the work-function (small difference with respect to the metallic tip) while yellow means higher absolute value of the work-function, indicative of an insulating state.

At 50 °C the surface potential is close to 0 mV (consistent with a metallic state), while at 30 °C the absolute value of the surface potential is high across the entire surface, consistent with an insulating phase. At 40 °C there is phase coexistence, with the phase boundaries between insulating and metallic regions coinciding with the cracks. The surface potential changes by about 0.2 ± 0.1 V between the low temperature (insulating) and the high temperature (metallic) phases. Taking the surface potential of our tip to be about 5 V,[38] this would represent a change in surface potential from 5.3 V (insulating) to 5.1 V (metal), in good agreement with prior studies.[34-37]

These observations indicate that each domain transits independently from the others, acting as separate units. Cracks thus act as natural barriers that isolate each domain from its neighbors, and such confinement means that it is, in principle, possible to modify the electronic properties of each individual domain.

Figure 4b reveals the result of illuminating an area of our films with a laser (λ = 488 nm; power = 3 mW; exposition = 1 min). It can be seen that the illuminated area has become darker, indicating the transition to the metallic phase. Importantly, each illuminated domain is darker towards the middle but remains unswitched (insulating) towards its edges (the relaxed region surrounding the cracks). In other words, each domain behaves de facto like a separate pixel.

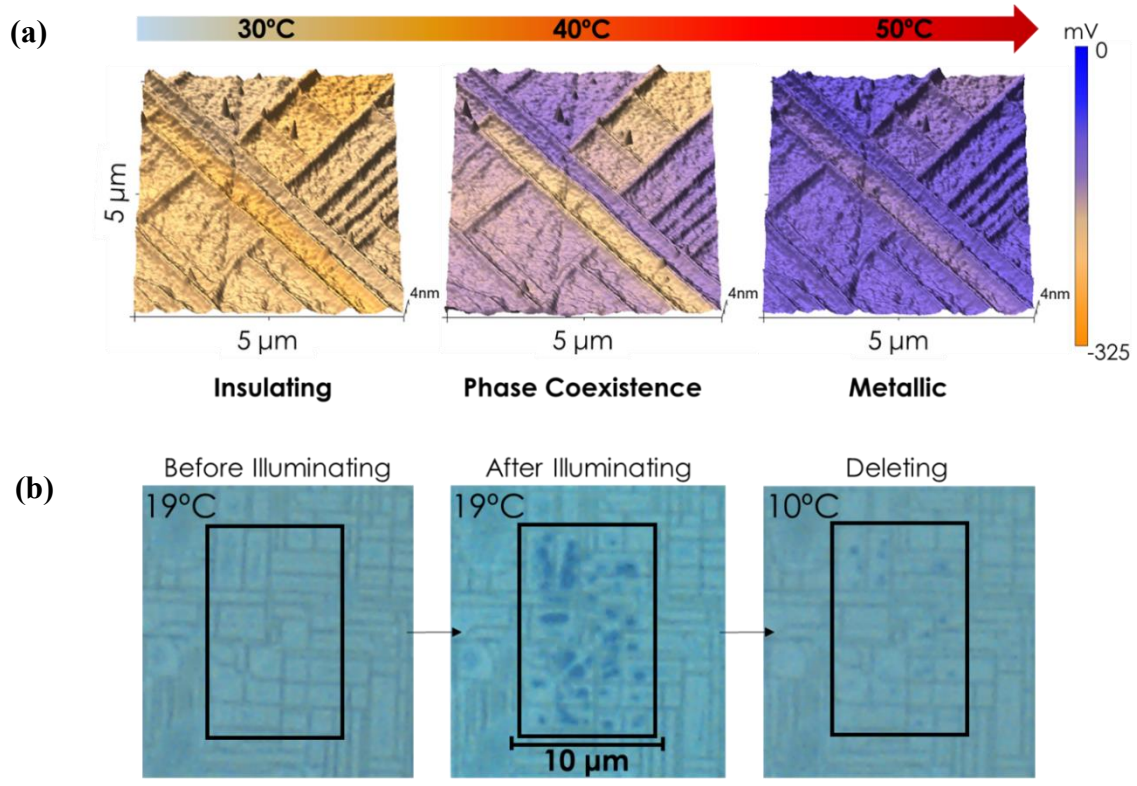

Figure 4. Self-confinement of MIT. (a) SKPM images at 30 °C, 40 °C and 50 °C (from left to right) showing the local MIT of a 20 nm-thick VO_2 film. (b) Optical writing. Optical images of reversible photo-induced MIT. With the film in the insulating phase, we wrote metallic (dark) domains by illuminating a spot with a 488 nm blue laser. The domains could be deleted (returning them to the insulating ground state) by cooling below T_{MI}.

It is also possible to induce the metal-insulator transition by applying an electric field, because charge-injection increases the charge-carrier density and favors the metallic state.[2,6,39-41] Here we inject charge by applying a voltage to the conducting-tip of an AFM in contact with an individual domain (**Figure 5**a). The schematic of the experiment and the main results are shown in **Figure 5**. We used a "self-pixelated" VO_2 film of 85 nm grown on insulating TiO_2(001). The surface of the film was grounded, so the surface potential values have an opposite sign from the ones in **Figure 4**a. We measured the surface potential inside and outside an individual island-domain, before and after applying voltage to the AFM tip. The charge-injection and its relaxation behavior were characterized as a function of temperature and time with a fixed voltage (1 V), and also as a function of both voltage and time at RT (**Figure 5**c).

As temperature increases with no voltage applied, VO_2 transits into the metallic state (**Figure 5**b) and the absolute value of the surface potential decreases (**Figure 5**c), consistent with what was also observed in **Figure 4**a for a different film. In the metallic state at temperatures higher than 40 °C, delivering a voltage to the tip has no effect on the surface potential because the film's free carriers screen the tip voltage. At 35 °C or lower temperatures, however, the domain is in the insulating state and applying voltage to the tip does result in charge-injection or extraction from it, as evidenced from the induced change in surface potential.

VO_2 is an *n*-type conductor,[42] so negative voltage injects electrons, increases charge density and pushes the domain towards the metallic state. This shift is evidenced as a lowering of the surface potential after application of negative voltage; the surface potential in a domain written

with V = -3 V at RT is the same as that of the high-temperature metallic state. In contrast, positive voltage has the opposite effect of extracting electrons, thereby pushing the already insulating domain into even higher surface potential. In both cases, the voltage-induced changes relax back over time towards the insulating ground state, with exponential time constants sufficiently long (from 6 to 17 minutes depending on temperature and voltage) for the induced changes to be measurable even by such slow means as scanning probe microscopy.

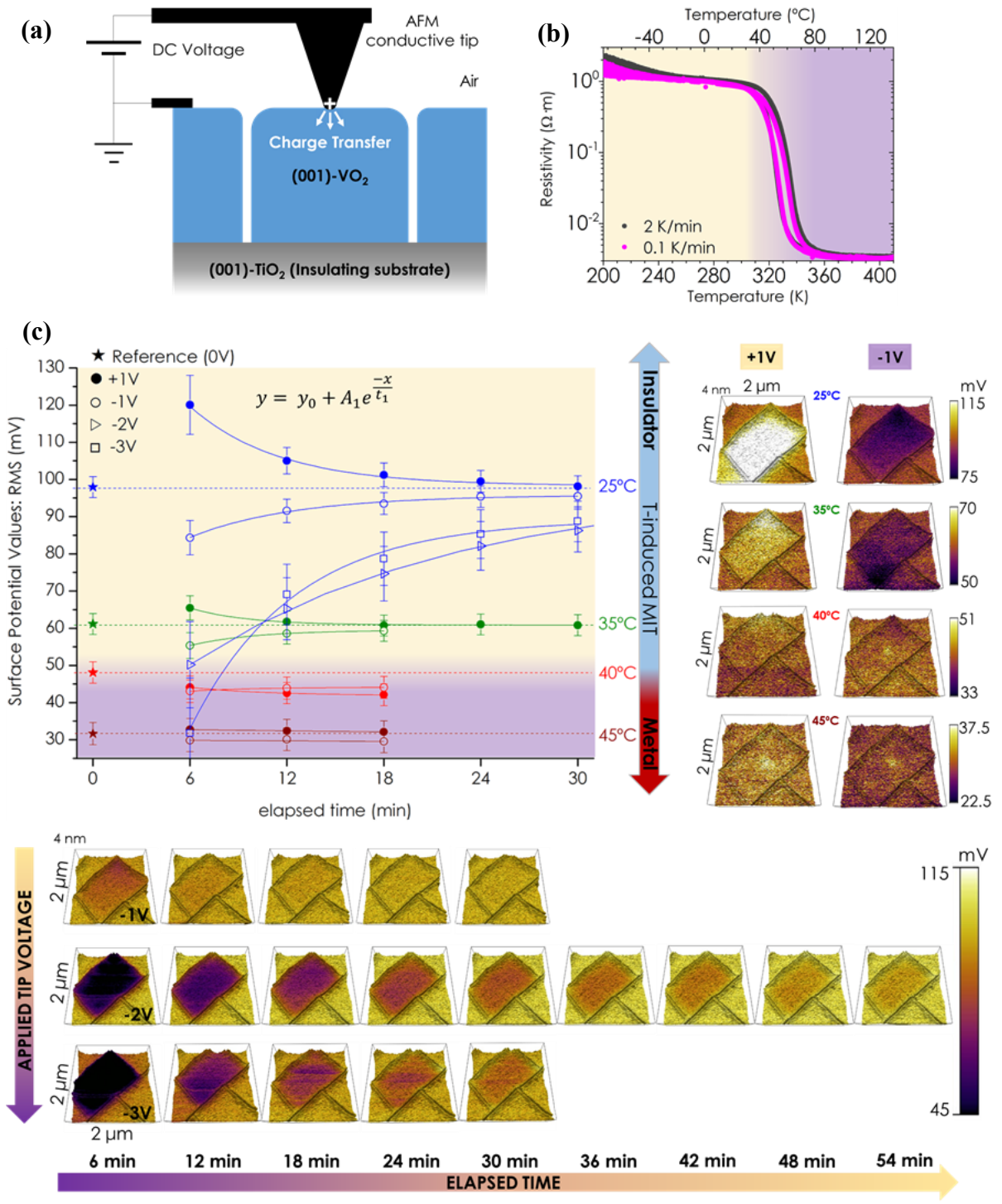

Figure 5. Charge-injection into a self-isolated "bit" and its characterization. (a) Scheme of the SKPM experiment to study charge-storage in VO_2. When the AFM tip contacts the domain's surface a DC voltage is applied to the tip during 10 s. Once the tip is withdrawn, the tip voltage

switches off to 0 V, and a surface potential scan is started immediately. (b) Temperature-dependent resistivity of the sample used for the experiment, measured using the temperature rates of 2 K/min (grey curve) and 0.1 K/min (pink curve). The resistivity drop starts ~ 40 ºC. The experiment results are represented in (c), where the surface potential RMS values are plotted versus both the temperature and the applied tip voltage. Some of the AFM images used for the analysis are shown.

The transition is not caused by thermal effects (Joule heating from leakage currents), since Joule heating would favor the high-temperature metallic phase for both voltage polarities, whereas we observe that positive voltages favor the insulating phase. Moreover, the thermalization time constant in thin films should be much faster (microseconds) than the long timescale (minutes) of our measurements, so any heating during the application of the voltage will disappear almost as soon as the voltage is switched off for the Kelvin-probe measurements. The electrostatic origin of the effect is also consistent with the magnitude of the electric field: if we simplify the AFM tip as a conductive sphere with a radius of 50 nm, a voltage of -2 V generates a radial electric field of the order of $\sim 40 \cdot 10^6$ V/m at the contact region, which is of the same order as the reported critical electric fields for inducing the MIT, 10^6-10^7 V/m.[39]

Cracking signifies a loss of mechanical integrity and is thus a source of device failure, so it is often studied with a preventive perspective. In recent times, however, cracking is also being embraced as a strategy for device nano-patterning.[43]

The self-patterned array of VO_2 is not perfectly regular, and pre-patterning (pre-etching) of the substrates is likely to be necessary in order to achieve perfect registry as required for memory

arrays. On the other hand, some irregularity in the registry is an advantage for photographic applications, as it naturally gets rid of the Moiré fringing artifacts that are inherent to regular CMOS and CCD photographic sensors. Thus, while both memory and pixel arrays made of self-patterned VO_2 are still far from actual real-world applicability, we believe the latter to be more hopeful.

The self-patterned VO_2 films can also be seen as a barrier-layer capacitor system, with the metallic domains behaving as floating electrodes and the insulating boundaries acting as the dielectric. This is reminiscent of other spontaneous barrier layer capacitor systems (Maxwell-Wagner capacitors) such as $CaCu_3Ti_4O_{12}$[44] or $CdCr_2S_4$[45]. On the other hand, the increased capacitance of VO_2 would only be in-plane, plus the leakage of VO_2 is too high to be of practical use as a barrier layer capacitor, leaving perhaps high-frequency applications with in-plane inter-digitated electrodes as the only capacitive functionality worth exploring.

V. CONCLUSIONS

VO_2 films thicker than 15 nm, grown on rutile $TiO_2(001)$, relax the epitaxial strain mainly by cracking following the $<110>_R$ crystallographic directions. It results in a rectangular pattern of VO_2 domains that may be addressed independently of each other. The material adjacent to a fissure relaxes locally (thus, T_{MI} ~ bulk VO_2), while the inner region of the VO_2 domain remains strained (lower T_{MI}). It leads to insulating-monoclinic strips of VO_2 framing metallic-rutile pads of VO_2. It has been shown that by either charge injection or optical excitation it is possible to induce the MIT at the VO_2 strained pads.

In epitaxial VO_2/TiO_2 thin films, fracture is all but inevitable above ~15 nm, but the ensuing pattern combined with the distinct electronic and optical properties that decorate the boundaries suggest that fracture may be constructively harnessed. From a functional point of view, the self-fractured films behave *de facto* as arrays of separate switchable elements: bits of information in a memory matrix or pixels in a photosensor array.

The bottom line is that, while still far from technological maturity, the regularity and distinct functionality of self-fractured epitaxial VO_2 films opens up new venues for applied exploration.

ASSOCIATED CONTENT

Supporting Information.

Detailed characterizations of structure, macroscopic electrical transport and surface besides experimental methods (PDF).

Animation of structural and metal-insulator transition measured simultaneously (ZIP).

AUTHOR INFORMATION

Corresponding Author

*E-mail: laura.rodriguez@icn2.cat

ACKNOWLEDGMENT

This work was supported from the Spanish Ministry of Economy, Industry and Competitiveness (project: MAT2016-77100-C2-1-P), the Catalan AGAUR agency for 2017SGR

and from Science Foundation Ireland (SFI 16/US/3344). ICN2 is funded by the CERCA programme/Generalitat de Catalunya and by the Severo Ochoa programme (SEV-2017-0706). LR particularly acknowledges the support of Severo Ochoa programme and ICN2 for her PhD grant, EDC acknowledges the Spanish "Juan de la Cierva" grant (JC-2015-25201) and the research project FIS2017-85787 and MC acknowledges funding from SFI Industry Fellowship (18/IF/6282).

VI. REFERENCES

(1) Berglund, C. N.; Guggenheim, H. J. Electronic properties of VO2 near the semiconductor-metal transition. *Phys. Rev.* **1969**, *185*, 1022 – 1033.

(2) Stefanovich, G.; Pergament, A.; Stefanovich, D. Electrical switching and Mott transition in VO2. *J. Phys.: Condens. Matter* **2000**, *12*, 8837.

(3) Yang, Z.; Ko, C.; Ramanathan, S. Oxide electronics utilizing ultrafast metal-insulator transitions. *Annu. Rev. Mater Res.* **2011**, *41*, 337 – 367.

(4) Liu, M.; Hwang, H. Y.; Tao, H.; Strikwerda, A. C.; Fan, K.; Keiser, G. R.; Sternbach, A. J.; West, K. G.; Kittiwatanakul, S.; Lu, J.; Wolf, S. A.; Omenetto, F. G.; Zhang, X.; Nelson, K. A.; Averitt, R. D. Terahertz-field-induced insulator-to-metal transition in vanadium dioxide metamaterial. *Nature* **2012**, *487*, 345 – 348.

(5) Aetukuri, N. P.; Gray, A. X.; Drouard, M.; Cossale, M.; Gao, L.; H. Reid, A.; Kukreja, R.; Ohldag, H.; Jenkins, C. A.; Arenholz, E.; Roche, K. P.; Durr, H.; G. Samant, M.; Parkin, S.

Control of the metal–insulator transition in vanadium dioxide by modifying orbital occupancy. *Nat. Phys.* **2013**, *9*, 661 – 666.

(6) Chen, F.H.; Fan, L. L.; Chen, S.; Liao, G. M.; Chen, Y. L.; Wu, P.; Song, L.; Zou, C. W.; Wu, Z. Y. Control of the metal–insulator transition in VO2 epitaxial film by modifying carrier density. *ACS Appl. Mater. Inter.* **2015**, *7*, 6875 – 6881.

(7) Nakano, M.; Shibuya, K.; Okuyama, D.; Hatano, T.; Ono, S.; Kawasaki, M.; Iwasa, Y.; Tokura, Y. Collective bulk carrier delocalization driven by electrostatic surface charge accumulation. *Nature* **2012**, *487*, 459 – 462.

(8) Ke, Y.; Wang, S.; Liu, G.; Li, M.; White, T.J.; Long, Y. Vanadium dioxide: the multistimuli responsive material and its applications. *Small* **2018**, *14*, 1802025.

(9) Yajima, T.; Nishimura, T.; Toriumi, A. Positive-bias gate-controlled metal–insulator transition in ultrathin VO2 channels with TiO2 gate dielectrics. *Nat. Commun.* **2015**, *6*, 10104.

(10) Zhou, Y.; Ramanathan, S. GaN/VO2 heteroepitaxial pn junctions: Band offset and minority carrier dynamics. *J. Appl. Phys.* **2013**, *113*, 213703.

(11) Kasırga, T. S.; Sun, D.; Park, J. H.; Coy, J. M.; Fei, Z.; Xu, X.; Cobden, D. H. Photoresponse of a strongly correlated material determined by scanning photocurrent microscopy. *Nat. Nanotechnol.* **2012**, 7, 723.

(12) Wentzcovitch, R. M.; Schulz, W. W.; Allen, P. B. VO2: Peierls or Mott-Hubbard? A view from band theory. *Phys. Rev. Lett.* **1994**, *72*, 3389 – 3392.

(13) Eyert, V. The metal-insulator transitions of VO2: A band theoretical approach. *Ann. Phys.* **2002**, *11*, 650 – 704.

(14) Liu, W.-T.; Cao, J.; Fan, W.; Hao, Z.; Martin, M. C.; Shen, Y. R.; Wu, J.; Wang, F. Intrinsic optical properties of vanadium dioxide near the insulator−metal transition. *Nano Lett.* **2011**, *11*, 466 – 470.

(15) Chen, S.; Liu, J.; Luo, H.; Gao, Y. Calculation evidence of staged Mott and Peierls transitions in VO2 revealed by mapping reduced-dimension potential energy surface. *J. Phys. Chem. Lett.* **2015**, *6*, 3650 – 3656.

(16) Gregg, J. M.; Bowman, R. M. The effect of applied strain on the resistance of VO2 thin films. *Appl. Phys. Lett.* **1997**, *71*, 3649 – 3651.

(17) Fan, L. L.; Chen, S.; Luo, Z. L.; Liu, Q. H.; Wu, Y. F.; Song, L.; Ji, D. X.; Wang, P.; Chu, W. S.; Gao, C.; Zou, C. W.; Wu, Z. Y. Strain dynamics of ultrathin VO2 film grown on TiO2 (001) and the associated phase transition modulation. *Nano Lett.* **2014**, *14*, 4036 – 4043.

(18) Kittiwatanakul, S.; Wolf, S. A.; Lu, J. Large epitaxial bi-axial strain induces a Mott-like phase transition in VO2. *Appl. Phys. Lett.* **2014**, *105*, 073112.

(19) Cui, Y.; Ramanathan, S. Substrate effects on metal-insulator transition characteristics of rf-sputtered epitaxial VO2 thin films. *J. Vac. Sci. Technol. A* **2011**, *29*, 041502.

(20) Yang, M.; Yang, Y.; Hong, B.; Wang, L.; Hu, K.; Dong, Y.; Xu, H.; Huang, H.; Zhao, J.; Chen, H.; Song, L.; Ju, H.; Zhu, J.; Bao, J.; Li, X.; Gu, Y.; Yang, T.; Gao, X.; Luo, Z.; Gao, C. Suppression of structural phase transition in VO2 by epitaxial strain in vicinity of metal-insulator transition. *Sci. Rep.* **2016**, *6*, 23119.

(21) Nagashima, K.; Yanagida, T.; Tanaka, H.; Kawai, T. Stress relaxation effect on transport properties of strained vanadium dioxide epitaxial thin films. *Phys. Rev. B* **2006**, *74*, 172106.

(22) Kawatani, K.; Kanki, T.; Tanaka, H. Formation mechanism of a microscale domain and effect on transport properties in strained VO2 thin films on TiO2(001). *Phys. Rev. B* **2014**, *90*, 054203.

(23) Li, X.; Gloter, A.; Gu, H.; Cao, X.; Jin, P.; Colliex, C. Role of epitaxial microstructure, stress and twin boundaries in the metal–insulator transition mechanism in VO2/Al2O3 heterostructures. *Acta Mater.* **2013***, 61*, 6443 – 6452.

(24) Balakrishnan, V.; Ko, C.; Ramanathan, S. In situ studies on twinning and cracking proximal to insulator–metal transition in self-supported VO2/Si3N4 membranes. *J. Mater. Res.* **2012**, *27*, 1476 – 1481.

(25) Fisher, B.; Patlagan, L. Switching VO2 Single Crystals and Related Phenomena: Sliding Domains and Crack Formation. *Materials*, **2017**, *10*, 554.

(26) Thouless, M. D. Crack spacing in brittle films on elastic substrates. *J. Am. Ceram. Soc.* **1990**, *73*, 2144 – 2146.

(27) Huang, Y.; Zhang, L.; Guo, T.; Hwang, K.-C. Mixed mode near-tip fields for cracks in materials with strain-gradient effects. *J. Mech. Phys. Solids* **1997**, *45*, 439 – 465.

(28) Cavalleri, A.; Tóth, C.; Siders, C. W.; Squier, J. A.; Ráksi, F.; Forget, P.; Kieffer, J. C. Femtosecond Structural Dynamics in VO2 during an Ultrafast Solid-Solid Phase Transition. *Phys. Rev. Lett.* **2001**, *87*, 237401.

(29) Zhou, Y.; Chen, X.; Ko, C.; Yang, Z.; Mouli, C.; Ramanathan, S. Voltage-triggered ultrafast phase transition in vanadium dioxide switches. IEEE Electr. Device L. **2013**, *34*, 220 – 222.

(30) Catalan, G.; Bowman, R.; Gregg, J. Metal-insulator transitions in NdNiO3 thin films. *Phys. Rev. B* **2000**, *62*, 7892.

(31) Abbate, M.; de Groot, F. M. F.; Fuggle, J. C.; Ma, Y. J.; Chen, C. T.; Sette, F.; Fujimori, A.; Ueda, Y.; Kosuge, K. Soft-x-ray-absorption studies of the electronic-structure changes through the VO2 phase transition. *Phys. Rev. B* **1991**, *43*, 7263 – 7266.

(32) Gray, A. X.; Jeong, J.; Aetukuri, N. P.; Granitzka, P.; Chen, Z.; Kukreja, R.; Higley, D.; Chase, T.; Reid, A. H.; Ohldag, H.; Marcus, M. A.; Scholl, A.; Young, A. T.; Doran, A.; Jenkins, C. A.; Shafer, P.; Arenholz, E.; Samant, M. G.; Parkin, S. S. P.; Dürr, H. A. Correlation-driven insulator-metal transition in near-ideal vanadium dioxide films. *Phys. Rev. Lett.* **2016**, *116*, 116403.

(33) Koethe, T. C.; Hu, Z.; Haverkort, M. W.; Schüßler-Langeheine, C.; Venturini, F.; Brookes, N. B.; Tjernberg, O.; Reichelt, W.; Hsieh, H. H.; Lin, H.-J.; Chen, C. T.; Tjeng, L. H. Transfer of Spectral Weight and Symmetry across the Metal-Insulator Transition in VO2. *Phys. Rev. Lett.* **2006**, *97*, 116402.

(34) Sohn, A.; Kanki, T.; Tanaka, H.; Kim, D.-W. Visualization of local phase transition behaviors near dislocations in epitaxial VO2/TiO2 thin films. *Appl. Phys. Lett.* **2015**, *107*, 171603.

(35) Sohn, A.; Kim, H.; Kim, D.-W.; Ko, C.; Ramanathan, S.; Park, J.; Seo, G.; Kim, B.-J.; Shin, J.-H.; Kim, H.-T. Evolution of local work function in epitaxial VO2 thin films spanning the metal-insulator transition. *Appl. Phys. Lett.* **2012**, *101*, 191605.

(36) Sohn, A.; Kanki, T.; Sakai, K.; Tanaka, H.; Kim, D.-W. Fractal Nature of Metallic and Insulating Domain Configurations in a VO2 Thin Film Revealed by Kelvin Probe Force Microscopy. *Sci. Rep.* **2015**, *5*, 10417.

(37) Ko, C.; Yang, Z.; Ramanathan, S. Work Function of Vanadium Dioxide Thin Films Across the Metal-Insulator Transition and the Role of Surface Nonstoichiometry. *ACS Appl. Mater. Inter.* **2011**, *3*, 3396 – 3401.

(38) Kaja, K. Development of nano-probe techniques for work function assessment and application to materials for microelectronics. Ph.D Thesis, Université Joseph-Fourier - Grenoble I, September 2010.

(39) Ruzmetov, D.; Gopalakrishnan, G.; Deng, J.; Narayanamurti, V.; Ramanathan, S. Electrical triggering of metal-insulator transition in nanoscale vanadium oxide junctions. *J. Appl. Phys.* **2009**, *106*, 083702.

(40) Chae, B.-G.; Kim, H.-T.; Youn, D.-H.; Kang, K.-Y. Abrupt metal–insulator transition observed in VO2 thin films induced by a switching voltage pulse. *Physica B* **2005**, *369*, 76 – 80.

(41) Li, Z.; Wu, J.; Hu, Z.; Lin, Y.; Chen, Q.; Guo, Y.; Liu, Y.; Zhao, Y.; Peng, J.; Chu, W.; Wu, C.; Xie, Y. Imaging metal-like monoclinic phase stabilized by surface coordination effect in vanadium dioxide nanobeam. *Nat. Commun.* **2017**, *8*, 15561.

(42) Zhou, Y.; Ha, S. D.; Ramanathan, S. Computation and learning with metal-insulator transitions and emergent phases in correlated oxides. In Cmos and Beyond: Logic Switches For Terascale Integrated Circuits; Liu, T.-J. K., Kuhn, K., Eds.; Electronic, optoelectronic devices, and nanotechnology; Cambridge Univ. Press: Cambridge, 2015; pp 209-235.

(43) Nam, K. H.; Park, I.H.; Ko, S. H. Patterning by controlled cracking. *Nature* **2012**, *485*, 221.

(44) Sinclair, D. C.; Adams, T. B.; Morrison, F. D.; West, A. R. CaCu3Ti4O12: One-step internal barrier layer capacitor. *Appl. Phys. Lett*. **2002**, *80*, 2153-2155

(45) Catalan, G.; Scott, J. F. Is CdCr2S4 a multiferroic relaxor? *Nature* **2007**, *448*, E4-E5

ToC Graphic. For Table of Contents Only: